Title: Loss of Bcl6 transcriptionally alters classical dendritic cells and diminishes T follicular helper cell-inducing cDC2 in mouse spleen

Authors: Hongkui Xiao[1], Isabel Ulmert[1], Hamsa Narasimhan[2], Ilia Kurochkin[3,4], Urs Mörbe[1], Dirk Baumjohann[5], Filipe Pereira[3,4,6], Barbara U. Schraml[2,7], Katharina Lahl[1,8,*]

Affiliations:

[1]Section for Experimental and Translational Immunology, Institute for Health Technology, Technical University of Denmark (DTU), 2800 Kongens Lyngby, Denmark

[2]Biomedical Center, Institute of Cardiovascular Physiology and Pathophysiology, Faculty of Medicine, Ludwig-Maximillians-Universität München, Planegg-Martinsried, Germany.

[3]Cell Reprogramming in Hematopoiesis and Immunity Laboratory, Lund Stem Cell Center, Molecular Medicine and Gene Therapy, Lund University, Lund, Sweden.

[4]Wallenberg Center for Molecular Medicine, Lund University, Lund, Sweden.

[5]Medical Clinic III for Oncology, Hematology, Immuno-Oncology and Rheumatology, University Hospital Bonn, University of Bonn, Bonn, Germany.

[6]Center for Neuroscience and Cell Biology, University of Coimbra, Coimbra, Portugal.

[7]Walter-Brendel-Centre of Experimental Medicine, University Hospital, LMU Munich, Planegg-Martinsried, Germany

[8]Immunology Section, Lund University, Lund 221 84, Sweden

[*] Corresponding author: Katharina Lahl (katharina.lahl@med.lu.se)

Keywords: dendritic cells, transcriptional regulation, Bcl6, cDC1, cDC2

Abstract

Dendritic cells express the transcriptional repressor Bcl6, but its precise role in the development and function within the dendritic cell (DC) compartment has been heavily debated. Here we show changes in phenotypes but preservation in cDC1 and cDC2 lineage identity in mice lacking Bcl6 specifically in cDC1 or all DCs. Spleen and lymph node (LN) resident cDC1 numbers are unchanged in the absence of Bcl6, while numbers of intestinal cDC1 and their migratory counterparts in the

mesenteric LN (mLN) are decreased, suggesting local differences regarding the impact of Bcl6 deficiency. Although Bcl6-deficiency affected the expression of many genes, cDC1 maintained their ability to cross-present antigen to $CD8^+$ T cells. Surprisingly, the absence of Bcl6 in DCs caused a complete loss of Notch2-dependent $ESAM^{hi}$ cDC2 in the spleen. Accordingly, DC-targeted Bcl6-deficient mice induced fewer T follicular helper cells in response to the model antigen ovalbumin. Our findings establish Bcl6 as an essential transcription factor for a subset of cDC2 and add to our understanding of the transcriptional landscape underlying cDC2 heterogeneity.

One Sentence Summary: Deficiency in the transcription factor Bcl6 dendritic cells alters the transcriptional profile of cDC1 and causes a specific loss of $ESAM^{hi}$ cDC2 in the murine spleen.

Main Text:

INTRODUCTION

Conventional dendritic cells (cDCs) have the unique ability to present antigen to naïve T cells of the adaptive immune system within lymphoid organs[1–3]. Upon encounter of antigen, migratory DCs scanning the peripheral environment mature and relocate to the draining LNs, where they collaborate with LN-resident DCs to initiate immunity[4]. The spleen is the secondary lymphoid organ responsible for induction of immune responses to blood-derived antigen[5]. A similar relocation of migratory DCs from the marginal zone and red pulp into the white pulp, where naïve B and T cells reside, occurs upon maturation of splenic DC subsets in this organ[6,7]. "Resident" resting DCs are also found in the spleen, where they are located in the T cell zones in the absence of stimulation[8].

Conventional DCs are broadly divided into two main subsets, cDC1 and cDC2[1]. cDC1 are characterized by their expression of the cDC1-exclusive chemokine receptor XCR1 and the absence of CD11b and Sirpα. Their development and functions are dependent on the transcription factors (TFs) IRF8[9,10], BATF3[11], Nfil3[12,13] and Id2[14] and they excel at cross-presenting antigen to CD8 T cells, which is at least in part attributable to their ability to engulf apoptotic

material[15–19]. cDC2 express high levels of CD11b and Sirpα, but not XCR1 and the transcriptional network governing their development is less well defined. IRF4-deficiency leads to a partial loss of cDC2 and is thought to impact primarily on their survival and ability to migrate[20–22]. Other TFs reported to influence cDC2 development or function include ZEB2[23], IRF-2[24] and Rel-B[25]. In the spleen, the majority of cDC2 express endothelial cell specific adhesion marker (ESAM), a marker defining cDC2 located in the bridging channels of the marginal zone, where they fulfill critical functions in activating CD4 T cells and germinal center (GC) formation[26,27]. The development of ESAM^{hi} cDC2 depends on Notch2-signaling induced by delta ligand 1 (DLL1) expressed by stromal cells[20,26,28,29] and on the chemokine receptor Ebi2 (GPR183)[30]. cDC2 show a higher level of heterogeneity than cDC1[31] and recent attempts to subset cDC2 further have suggested separation based on Notch2 versus Klf4-dependency[32], or on expression of the TFs Tbet (cDC2A) and RORγt (cDC2B)[33].

The TF Bcl6 plays an essential role in GC reactions, being required for the differentiation of both GC B cell and T follicular helper (T_{FH}) cells in a cell intrinsic manner[34]. Bcl6 is expressed in cDC1, and to a lower extent in cDC2[31] and we have shown previously that complete Bcl6-deficiency causes a loss of CD11b^{-} DCs, presumed to be cDC1[31]. Other work has confirmed that Bcl6-deficient mice lack splenic CD8-expressing cDC1, but also reported a reduction in splenic CD4^{+} cDC2[35]. However, a more recent study has disputed these findings, by showing normal cDC1 numbers in mice with conditional *Bcl6* deletion driven by cre recombinase under the control of the *Csf1* promoter. Importantly, these authors suggested that down-regulation of CD11c in the absence of Bcl6 may have compromised the detection of cDC1 in the earlier studies[36]. Here we have attempted to reconcile these conflicting data by performing in-depth analysis of the DC compartment in mice lacking Bcl6 in all DCs or specifically in cDC1, using CD11c- or XCR1- driven cre drivers respectively. Our results show that while cDC1 showed substantial alterations in gene expression including deregulation of genes involved in cytokine signaling and cell adhesion, their ability to cross-present antigen was largely conserved in the absence of Bcl6. However cross-presentation efficiency differed between organs and reflected previously neglected tissue-specific decreases in cDC1. Bcl6-deficiency in DC led to a complete loss of the Notch2-dependent ESAM^{hi} cDC2 subset in the spleen and consequently to a defect in splenic T_{FH} cell induction to

ovalbumin as a model antigen. Our findings suggest that the core subset identities of cDC1 and cDC2 are maintained in the absence of Bcl6, but that its deficiency in DCs causes intrinsic, subset-specific alterations in DC abundance and function.

RESULTS

Bcl6 deficiency alters DC subset phenotypes and numbers across tissues

We have shown previously that mice completely lacking Bcl6 are largely devoid of CD11b$^-$ DCs, presumed to be cDC1[31]. To better define the impact of Bcl6-deficiency on cDC1, we generated mice lacking Bcl6 specifically in cDC1 by crossing XCR1.cre mice to mice carrying a floxed Bcl6 gene (*XCR1.Bcl6^{KO}*). Additionally, we deleted Bcl6 in all CD11c-expressing cells by crossing CD11c.cre mice to Bcl6^{flox} mice (*CD11c.Bcl6^{KO}*). As controls, we used the relevant cre negative Bcl6^{flox} littermates (designated as wt throughout). As expected, flow cytometry revealed mutually exclusive populations of CD11c$^+$MHCII$^+$ cDC in the wt spleen based on the expression of XCR1 or CD11b to identify cDC1 and cDC2, respectively. However, there was a clear population of XCR1$^+$CD11b$^+$ DCs in the absence of Bcl6 in the spleen of both Bcl6-deficient mouse lines (Fig. 1A). XCR1$^+$CD11b$^+$ were also abundant within the resident populations of peripheral and mesenteric lymph node (pLN and mLN) DCs in the absence of Bcl6 (Fig. 1B). The absolute numbers of total XCR1$^+$ cDCs (independent of CD11b expression) were only mildly reduced in *XCR1.Bcl6^{KO}* and normal in *CD11c.Bcl6^{KO}* mice, while XCR1$^-$CD11b$^+$ DCs were significantly diminished in *CD11c.Bcl6^{KO}* mice, but normal in *XCR1.Bcl6^{KO}* mice (Fig. 1A). Resident DC populations were not substantially altered in either pLN or mLN (Fig. 1B).

We next analyzed migratory DC populations in different organs. Mice lacking Bcl6 in cDC1 or in all DCs had significantly fewer migratory XCR1$^+$ DCs in pLN and mLN and these also expressed CD11b (Fig. 2A). Interestingly, we also detected a loss of XCR1$^-$CD103$^+$CD11b$^+$ DCs in the migratory compartment of the mLNs of CD11c.Bcl6^{KO} mice, whereas the numbers of XCR1$^-$CD103$^-$CD11b$^+$ DCs were normal (Fig. 2A). As the majority of migratory DCs in the mLNs derives from the small intestinal lamina propria (SILP), we next analyzed this compartment. This showed there were fewer XCR1$^+$ DCs in the SILP of both *XCR1.Bcl6^{KO}* and *CD11c.Bcl6^{KO}* mice, all of which again

expressed CD11b (Fig. 2B). In addition, the numbers of XCR1$^-$CD103$^+$CD11b$^+$ DCs were reduced in *CD11c.Bcl6^{KO}* mice, while the numbers of XCR1$^-$CD103$^-$CD11b$^+$ DCs were less affected (Fig. 2B). Together these results suggest that the decreases in migratory XCR1$^+$ and XCR1$^-$CD103$^+$CD11b$^+$ DCs seen in mLN are caused by absence of these populations, rather than a deficiency in their ability to migrate. Similar changes in cDC were seen in the lung in the absence of Bcl6, with reduced numbers and upregulation of CD11b in XCR1$^+$ DCs in both *XCR1.Bcl6^{KO}* and *CD11c.Bcl6^{KO}* mice, together with reduced numbers of XCR1$^-$CD11b$^+$ DCs in *CD11c.Bcl6^{KO}* mice (Suppl. Fig. 1A). Thus, Bcl6 deficiency affects cDC in several locations.

As CD11c is expressed by other cells including macrophages[20], we verified our findings in mice in which Bcl6 deletion was induced by cre recombinase under the control of the *Clec9a* promoter, a system which targets both cDC1 and cDC2 and is selective to the cDC lineage[37]. These mice additionally carry a YFP reporter following a floxed stop cassette in the ubiquitous ROSA26 locus to monitor targeting efficiency. Virtually all remaining XCR1$^+$ DCs were positive for YFP, while only half of the XCR1$^-$ SILP DCs were YFP-labelled, suggesting only partial targeting efficiency using this model (Fig. 2C). We thus used YFP-expression as a surrogate for cre recombinase activity, and by extension Bcl6-deficiency. In agreement with our findings in *CD11c.Bcl6^{KO}* mice suggesting that Bcl6-deficiency results in fewer SILP CD103$^+$CD11b$^+$ DCs, the YFP$^-$ population contained a higher proportion of XCR1$^-$CD103$^+$CD11b$^+$ DCs than the YFP$^+$ population (Fig. 2C). Together, these data indicate that loss of Bcl6 has significant effects on both XCR1$^+$ and XCR1$^-$ DCs.

cDC1 and cDC2 signatures are preserved in the absence of Bcl6 in DCs

One of the most surprising findings from our studies was the expression of the cDC2 marker CD11b by the XCR1$^+$ cDC that remained in Bcl6-deficient mice. To determine whether this reflects acquisition of CD11b by cDC1, or cDC2 with aberrant XCR1 expression, we sorted bulk populations of splenic XCR1$^+$ DCs (independent of CD11b expression) and XCR1$^-$CD11b$^+$ DCs from wt, *XCR1.Bcl6^{KO}* and *CD11c.Bcl6^{KO}* mice for mRNA-sequencing (see Fig. 1A for gating). Principal component (PC) analysis showed that XCR1$^+$ DCs segregated from XCR1$^-$CD11b$^+$ DCs from all mouse models along PC axis 1, which accounted for 69% of the variance. This strongly supports

the idea that Bcl6-deficient cDC1 and cDC2 maintained overall lineage identity (Fig. 3A). Nevertheless, PC2 separated the populations on the basis of Bcl6 presence or absence, accounting for 13% of the variance and suggesting that Bcl6 has a significant impact on the gene transcription profile of both cDC1 and cDC2. Interestingly, cDC1 from *XCR1.Bcl6*^{KO} and *CD11c.Bcl6*^{KO} mice clustered closely and were separated from wt cDC1, while cDC2 in *CD11c.Bcl6*^{KO} mice segregated from those in *XCR1.Bcl6*^{KO} and wt mice, consistent with XCR1-cre being specific to cDC1 and indicating that Bcl6 regulates gene expression in both DC subsets in a cell-intrinsic manner. PC3 accounted for 4% of the variance and showed opposite directional bias in Bcl6-deficient cDC1 and cDC2. This suggests that Bcl6-mediated regulation of gene transcription may affect some targets in cDC1 and cDC2 differently (Fig. 3A).

To explore further how Bcl6 might regulate cDC lineage identity, we generated cDC1 and cDC2 signatures by identifying the top 50 genes that were differentially expressed between our wt cDC1 and cDC2 and interrogated how these signatures were affected by a loss of Bcl6 expression (for gene lists and expression levels see Suppl. Table 1). Supporting their maintenance of lineage identity, XCR1^{+} cDC from both *XCR1.Bcl6*^{KO} and *CD11c.Bcl6*^{KO} mice retained the expression of cDC1 markers, including *Irf8*, *Tlr3*, *Clec9a*, and *Cadm1* (Fig. 3B). However, *Cd8a* was downregulated in Bcl6-deficient XCR1^{+} cDC and several genes associated with cDC2 identity were upregulated by XCR1^{+} cDC in the absence of Bcl6, including *Sirp*α, *Zeb2*, *Csf1r* and *Itgam* (encoding CD11b) (foldchange > 2, padjust < 0.01). Although Bcl6-deficient CD11b^{+} cDC2 did not express cDC1 specific markers, cDC2 from *CD11c.Bcl6*^{KO} mice showed altered expression of several classical cDC2 markers, of which some were further upregulated such as *Csf1*, *Zeb2* and *Itgam*, while others were downregulated, including *Clec4a4* and *CD4* (Fig. 3B). Despite maintenance of core lineage expression patterns, the overall transcriptional profiles of XCR1^{+} and XCR1^{-}CD11b^{+} were significantly altered in the absence of Bcl6 (Fig. 3A, C). In total, 607 genes were differentially regulated in XCR1^{+} cDC from *XCR1.Bcl6*^{KO} mice compared with wt cDC1, with 473 being upregulated and 134 were downregulated. In contrast, of the 452 differentially regulated genes in cDC2 from *CD11c.Bcl6*^{KO} mice, only 206 were upregulated, compared with 246 downregulated genes (Fig. 3D, for list of contributing genes see Suppl. Table 2). Interestingly, only 79 genes were coordinately overexpressed in Bcl6-deficient cDC1 and cDC2, and 32 genes were

coordinately downregulated in the absence of Bcl6 in both subsets. 12 genes were reciprocally regulated in the two subsets, of which 11 genes were upregulated in cDC1 and downregulated in cDC2 (including receptor encoding genes *Ffar1* and *Lair1,* enzyme-encoding genes *Tgm2, Pigv* and *Malt1* and genes encoding proteins implicated in cellular and intracellular adhesion and transport *Cdh17, Ctnnd2, Ston2 and Rin2*). The gene for the actin-binding protein Plectin was the only gene upregulated in cDC2 and downregulated in cDC1. Taken together, although the lineage identity of splenic cDC1 and cDC2 is generally maintained in the absence of Bcl6, this does result in significant changes in subset-specific gene expression in both cDC subsets.

Bcl6-deficiency in cDC1 causes alterations in immunologically relevant pathways

To better characterize the impact of Bcl6-deficiency on cDC1, we first compared the expression of cDC1-related markers using flow cytometry. This confirmed the maintenance of TLR3, XCR1, IRF8, CD103 and CLEC9A expression by XCR1$^+$ cDC from the spleen of *XCR1.Bcl6^{KO}* mice, as well as upregulation of CD11b and Sirpα and loss of CD8α (Fig. 4A). In addition, we detected higher expression of the maturation marker CD24 on Bcl6-deficient cDC1, which together with the upregulated cytokine receptors and C-type lectin receptors may suggest an elevated activation status of Bcl6-deficient cDC1. Next, we analyzed how the absence of Bcl6 might influence the immunological functions of cDC1 by performing gene set enrichment analysis of the RNA-Seq data from XCR1$^+$ cDC in *XCR1.Bcl6^{KO}* and wt mice. This showed that several immunologically relevant gene ontology pathways were enriched within the differentially expressed gene sets, including *leukocyte adhesion*, *proliferation* and *activation*, and *production of IL-1* (Fig. 4B). In parallel, KEGG pathway analysis highlighted differences in *cytokine-cytokine receptor interactions, NOD-like receptor signaling pathway, MERK signaling pathway, hematopoiesis cell lineage, Tuberculosis* and *C-type lectin receptor signaling pathway* (Fig. 4C, D).

Bcl6-deficient cDC1 maintain the ability to cross-present antigen

The most characteristic property of cDC1 is to cross-present exogenous antigen to class I MHC-restricted CD8$^+$ T cells, a function which involves cell-surface receptors such as CLEC9A (DNGR1) that mediate the uptake of apoptotic cells[18,19]. Our gene expression analysis suggested that XCR1$^+$ cDC1 maintained the expression of *Clec9a* in the absence of Bcl6 and this was confirmed by flow cytometry (Fig. 4A). We therefore examined whether cross-presentation was intact in *XCR1.Bcl6^{KO}* animals by injecting heat-killed ovalbumin-expressing mouse embryonic fibroblasts (OVA-MEFs) into recipient mice adoptively transferred with OVA-specific CD8 T cells from OT-I mice. OT-I proliferation strictly depends on cDC1-mediated cross-presentation in this model[17]. OT-I cells proliferated to a similar extent in the spleens of OVA-MEF injected *XCR1.Bcl6^{KO}* and wt mice, suggesting that Bcl6-deficient cDC1 retain their ability to cross-present (Fig. 5A, B). The somewhat diminished proliferation in the mLN of *XCR1.Bcl6^{KO}* mice may reflect the decreased number of migratory cDC1 we found in the mLN of these mice (Fig. 2A).

Taken together, although cDC1-specific Bcl6 deficiency alters gene expression by cDC1, their overall numbers in the spleen and their ability to cross-present antigen in the spleen are largely unaffected.

Bcl6-deficiency results in a selective loss of Notch2-dependent cDC2

In addition to its role in cDC1, our initial results also revealed a significant role for Bcl6 in the gene expression signature of cDC2. Furthermore, the numbers of cDC2 were reduced in the spleen of *CD11c.Bcl6^{KO}* mice, as were the numbers of cDC2 expressing CD103 in the LP and MLN. Diminished cDC2 numbers in the blood of CD11c.Bcl6^{KO} mice suggest that this was not due to a release of cDC2 into the blood stream (Suppl. Fig. 1B). The remaining cDC2 in the spleen of *CD11c.Bcl6^{KO}* mice also showed somewhat lower expression of MHCII and higher expression of CD11b than wt cDC2 (Fig. 6A). Further phenotyping of spleen cDC2 in *CD11c.Bcl6^{KO}* mice revealed a striking loss of the ESAM^{hi} cDC2 subset (Fig 6B). Similar changes in CD11c and CD11b expression and loss of ESAM^{hi} DCs were also seen in *Clec9A.Bcl6^{KO}* mice (Fig. 6C, D). This was apparent in the analysis of bulk cDC2 in *Clec9A.Bcl6^{KO}* mice with a further pronounced phenotype detectable

when gating on YFP+ cDC2, presumably enriching for cDC2 with a history of *Clec9A*-promoter activity (Fig. 6D).

As described previously[26], the ESAM^{lo} subset of cDC2 expressed slightly lower levels of CD11c compared with their ESAM^{hi} counterparts and a significant proportion lacked expression of 33D1 and CD4 which were expressed uniformly by ESAM^{hi} cDC2 (Fig. 6E). The total population of cDC2 remaining in *CD11c.Bcl6^{KO}* mice resembled the ESAM^{lo} population in terms of these markers, but expressed higher levels of CD11b and IRF4 than either ESAM^{hi} or ESAM^{lo} wt cDC2 subset, suggesting these markers may be specific targets of Bcl6 repression.

To explore the nature of the cDC2 remaining in the spleen of *CD11c.Bcl6^{KO}* mice further, we compared their gene expression with publicly available bulk RNA-Seq data from ESAM^{hi} and ESAM^{lo} cDC2 from wt spleen[38] and compared differentially expressed genes with those reveled in CD11c.Bcl6^{KO} vs wt cDC2. As expected from their usual predominance in wt spleen, the majority of the top 50 genes expressed more prominently by ESAM^{hi} cDC2 were also significantly over-represented in our population of total wt cDC2, which expressed many fewer of the top 50 genes from ESAM^{lo} cDC2 (Fig. 7A). Conversely, the genes over-expressed by total cDC2 from *CD11c.Bcl6^{KO}* spleen showed much more overlap with the top 50 genes expressed by ESAM^{lo} cDC2, while the genes over-expressed by ESAM^{hi} cDC2 were mostly downregulated in Bcl6-deficient cDC2 (Fig. 7A, for a complete gene list containing expression levels see Suppl. Table 3). In total, 71 genes were coordinately expressed in ESAM^{hi} and wt cDC2, and 48 genes were coordinately expressed in ESAM^{lo} and Bcl6-deficient cDC2, while only one gene was upregulated in both ESAM^{hi} and Bcl6-deficient cDC2 and no genes were coordinately overexpressed in ESAM^{lo} and Bcl6-wt cDC2 (Fig. 7B, contributing genes listed in Suppl. Table 4). These data confirm that Bcl6 deficiency in DCs causes the loss of the ESAM^{hi} lineage of splenic cDC2.

ESAM^{+} spleen DCs are localized to the marginal zone bridging channels, where they play a prominent role in the induction of germinal center responses[27]. Confocal microscopy using CD11c as a pan-DC marker and TLR3 and Sirpα to define cDC1 and cDC2, respectively, confirmed a substantial loss of DCs from this region of *CD11c.Bcl6^{KO}* spleen (Fig. 7C). To test the functional relevance of this defect, we transferred wt and *CD11c.Bcl6^{KO}* mice with OT-II T cells, immunized

the mice with OVA + poly I:C intraperitoneally and assessed the generation of antigen-specific follicular helper T cells three days later. We chose this timepoint because this early T_{FH} cell induction is independent of GC B cells[39], which are known to express CD11c and are required for the maintenance of T_{FH} cells at later times[40]. Although OT-II cells expanded normally in the *CD11c.Bcl6*^{KO} mice in response to immunization, the early induction of antigen-specific T_{FH} cells was markedly reduced in immunized *CD11c.Bcl6*^{KO} mice compared with wt mice (Fig. 7D, E), suggesting that Bcl6-dependent cDCs indeed drive early T_{FH} induction in this model. Taken together, Bcl6 deficiency in the CD11c^{+} compartment causes the loss of cDC2 and affects the induction of adaptive immunity in the spleen.

DISCUSSION

We here show that Bcl6-deficiency in the DC compartment causes major transcriptional alterations with subset-specific consequences. cDC1 present with a XCR1/CD11b double-positive phenotype, markers mutually exclusive in a wt setting, where XCR1 defines cDC1 and CD11b defines cDC2. Genome-wide transcriptional analysis, in-depth cDC1 lineage marker assessment, and testing for cross-presentation ability clearly defined XCR1-expressing Bcl6-deficient DCs as cDC1, despite the prominent upregulation of CD11b. In-depth analysis of the splenic cDC2 compartment revealed that the ESAM^{hi} subset of cDC2 critically depends on Bcl6. Deficiency in Bcl6 specifically in DCs resulted in reduced splenic T_{FH} induction in response to protein antigen immunization, thus extending the role of Bcl6 in critically regulating all core immune cell types involved in the GC response also to the DC compartment.

We previously described a selective loss of splenic CD8α^{+}CD11b^{-} in Bcl6-deficient mice[31]. Here we refine this interpretation, describing that resident cDC1 numbers *per se* are not affected by the loss of Bcl6, but rather cDC1 upregulate CD11b and down-regulate CD8α, causing these cells to fall into the classical cDC2 gate. Numbers of migratory mLN and CD103^{+}CD11b^{-} intestinal cDC1 however are decreased in mice lacking Bcl6 within the DC compartment, a finding further supported by a local defect in cross presentation in the mLN. We currently cannot explain the differential effects of Bcl6 deficiency on resident versus migratory cDC1 populations.

Interestingly, this phenotype opposes what was recently described for DC-SCRIPT, absence of which selectively affected resident cDC1[41]. Since Bcl6 primarily acts as a transcriptional repressor, it is possible that DC-SCRIPT and Bcl6 integrate in a feedback loop to drive cDC1 migration or survival upon maturation, aspects which require further study.

DC progenitors in the bone marrow up to the pre cDC state were previously described to be negative for Bcl6 and consequently, DC precursor frequency is not affected by the lack of Bcl6[36,42]. This differs from other TFs implied in cDC1 lineage specification, such as IRF8, Nfil3, ZEB2 and Id2, placing Bcl6 downstream of these factors in the developmental cascade. Nfil3 was recently shown to suppress ZEB2 at the common DC precursor (CDP) stage, allowing for Id2 expression and cDC1 subset identity[13]. As Bcl6 deficiency in cDC1 does not impact on their lineage preservation despite prominent CD11b and ZEB2 upregulation, Bcl6 might fine-tune cDC1 identity by suppressing selected cDC2 genes at the mature state. As such, Bcl6-deficient cDC1 maintain key cDC1 genes such as XCR1, TLR3, and CLEC9A as well as cross-presentation functionality, but meanwhile present with a gene expression profile suggesting a "gain-of-function", including enhanced expression of genes of the cytokine-cytokine receptor pathway, cell adhesion and migration pathways and pathways associated with inflammasome activity, the latter commonly associated with cDC2. Exploring the functional implications of this on homeostasis and immunity is an interesting avenue for future research.

CD11c.Bcl6^{KO} and Clec9a.Bcl6^{KO} mice lacked the dominant subset of ESAM^{hi} cDC2 in the spleen, a phenotype reminiscent of Notch2 deficiency in DCs. Indeed, CD103^{+}CD11b^{+} SILP DCs were also affected in CD11c.Bcl6^{KO} and Clec9a.Bcl6^{KO} mice, again mirroring the phenotype observed in Notch2-deficient cDC2[20,26]. Splenic T_{FH} cell induction is reduced in CD11c.Bcl6^{KO} mice, functionally mimicking the phenotype of DC-specific Notch2-deficient mice. This may suggest that incorrect positioning prevents access to antigen, as has been previously discussed in Notch2-targeted models[26], or that development and/or survival of ESAM^{hi} cDC2 depend on correct positioning. Splenic cDC2 deficient in the homing receptor GPR183 fail to localize to the marginal zone bridging channels, resulting in lower homeostatic numbers on splenic cDC2 and an inability to mount adaptive immunity to blood-derived particulate antigen[43,44]. Bcl6 regulates GPR183 expression in B cells. However, GPR183 expression levels were not altered in Bcl6-deficient cDC2,

suggesting that either additional factors to GPR183 are required for the correct positioning of cDC2 in the spleen, or that Bcl6-deficiency causes a development block or diminished survival within ESAM^{hi} cDC2 that is irrespective of localization.

Comparison of gene expression profiles between ESAM^{hi} and ESAM^{lo} wt cDC2 subsets and cDC2 from CD11c.Bcl6^{KO} mice confirmed the alignment between ESAM^{lo} and Bcl6-deficient cDC2. The overlap was however only partial, suggesting that while Bcl6-deficiency causes the loss of the ESAM^{hi} subset, transcriptional changes occur in all cDC2. For example, the extent of deregulation of IRF4 and CD11b in the absence of Bcl6 cannot solely be explained by the loss of ESAM^{hi} cDC2. In addition, both markers are also upregulated in Bcl6-deficient cDC1. It remains possible that overlaps in the phenotype of Notch2-deficient and Bcl6-deficient DC compartment exceed the effects on ESAM^{hi} cDC2 as CD8α^{+}CD11b^{-} cDC1 are diminished in both mouse models (this study and [26,31,35]). We now show that in the absence of Bcl6, this reflects a change in phenotype and not the absence of the subset. Whether this is also the case in Notch2-deficient cDCs has not been assessed. Of note, the cDC1 maturation marker CD24 is upregulated in both Bcl6- and Notch2-targeted mice (our study and [20,26]), arguing against a developmental defect within the cDC1 spleen compartment also in Notch2-targeting models. It will be of great interest to further delineate if, where and how the Notch2-signaling pathway may intersect with Bcl6-regulated gene expression in DCs and to which extent this regulation is specific to the DC subset. Transcriptional changes within the Bcl6-deficient cDC2 compartment are dominated by the lack of the ESAM^{hi} subset. This possibly explains why many genes are down-regulated in Bcl6-deficient cDC2 despite its role as a transcriptional repressor.

We report here that Bcl6 deficiency maintains general cDC1 and cDC2 lineage identity, but markedly alters the transcription profile and tissue-specific abundance of both lineages. cDC1 present with an aberrant phenotype previously described in a model overexpressing the TF ZEB2 from the pre-cDC stage onwards[23]. This differs substantially from the previously described loss of cDC1 identity caused by the absence of the -32kb enhancer of IRF8, BATF3, or DC-SCRIPT[41,45]. In those models, all affecting the cDC1 lineage on the precursor level, specific cDC1 markers such as IRF8, TLR3, XCR1 and CLEC9A as well as their ability to cross-present antigen were impacted, hallmarks that are preserved in Bcl6-deficient cDC1. This suggests that Bcl6 may act downstream

of important lineage preserving factors by repressing few selected cDC2 specific markers in mature DCs in addition to a set of genes not implied in subset identity. Surprisingly, Bcl6-deficiency within the DC compartment caused a prominent loss of Notch2-dependent ESAM^{hi} spleen cDC2 with significant functional consequences for adaptive immunity towards a model antigen. The well accepted heterogeneity within the cDC2 compartment is to date poorly understood. Our data add to the emerging picture of transcriptional regulation of DC subsets by establishing that ESAM^{hi} cDC2 require Bcl6 in addition to Notch2- and lymphotoxin β-signaling for their development. Our findings establish Bcl6 as a subset-specific regulator of DC development and function with critical consequences for adaptive immune induction.

MATERIALS AND METHODS

Mice

Xcr1.cre (*B6-Xcr1^{tm2Ciphe}*)[46], *CD11c.cre*[29] and *Clec9A.cre*[37] mice were crossed to *Bcl6$^{fl/fl}$* mice[47] to obtain DC-specific Bcl6-knockout models. *Clec9A.Bcl6^{KO}* mice additionally contained a ROSAfloxSTOPflox-YFP allele. Mice were maintained heterozygous for cre and negative littermates were used as wt controls. Additional strains used in this study were B6.SJL-Ptprc^{a} Pepc^{b}/BoyJ (congenic C57BL/6.CD45.1 mice from the Jackson Laboratory), C57BL/6-Tg (Tcra Tcrb)1100Mjb/J and B6.Cg-Tg(TcraTcrb)425Cbn/J (OT-I and OT-II mice from Jackson Laboratory). Mice were group-housed in individually ventilated cages and maintained under specific pathogen-free conditions. Male and female littermates were used between 8 and 15 weeks of age, RNA-Seq was performed on female mice only. Breeding was performed in house at the BioF facility at DTU. All experiments were approved by the Danish Animal Experiments Inspectorate.

Cell preparation

Spleens, mesenteric LNs and peripheral LNs (axillary, brachial and inguinal) were digested in RPMI containing 5% FCS, 0.5 mg/ml Collagenase IV and 15 µg/ml DNase I for 45 min at room

temperature. Red blood cells in spleen and blood samples were subsequently lyzed using red blood cell lysis buffer (ammonium chloride, potassium bicarbonate, EDTA, and MiliQ water) for 3 minutes at room temperature.

Single cell suspensions of the SILP were prepared as previously described[48]. Briefly, the intestines were flushed with HBSS supplemented with FCS (10 %), Peyer's patches were removed and epithelial cells and mucus were removed by incubating tissue in HBSS supplemented with FCS (10%) and EDTA (2 mM) 3 times each for 15 min at 37 °C with continual shaking at 450 rpm. Remaining tissue pieces were digested in R10 media (RPMI 1640 supplemented with FCS (10 %) containing DNase I grade II (30 µg/ml) and Liberase TM (58 µg/ml, Roche) for 20 min at 37 °C with a magnetic stirrer.

Lungs were perfused with PBS prior to resection. All lung lobes were manually cut into small pieces and digested in R5 media (RPMI 1640 supplemented with FCS (5 %) containing DNase I grade II (30 µg/ml) and Liberase TM (50 µg/ml, Roche) for 45 min at 37 °C with a magnetic stirrer.

SILP and lung cell suspensions were filtered through 100-µm cell strainers (Fisher Scientific) and lymphocytes were enriched by density gradient centrifugation with 40 % / 70 % Percoll (GE Healthcare) prior to further analysis.

Flow cytometry

Single-cell suspensions were stained for multicolor analysis with the indicated fluorochrome- or biotin-conjugated antibodies after blocking with Fc block (purified anti-CD16/32). Antibodies were diluted in FACS buffer (DPBS, 2% FCS) and staining was performed for 30 min on ice in the dark. LIVE/DEAD™ Fixable Near-IR Dead Cell Stain Kit (Invitrogen) or Fixable Viability Dye eFluor™-780 (Invitrogen) were used for determining the viability of cells. For intracellular staining, cells were fixed with the Foxp3 Fixation/Permeabilization kit from eBioscience. Samples were acquired on a Fortessa X20 (BD) flow cytometer using FACSDiva software (BD Biosciences)

and further analyzed with FlowJo software (Tree Star). The following antibodies were used: PE-Cy7 anti-mouse NK1.1 (clone PK136), PE-Cy7 anti-mouse CD3 (clone 145-2C11), PE-Cy7 anti-mouse B220 (clone RA3-6B2), PE-Cy7 anti-mouse CD19 (clone eBio1D3), PE-Cy7 anti-mouse CD64 (clone X54-5/7.1), APC/BV711 anti-mouse CD11c (clone N418/HL3), FITC anti-mouse MHC-II (clone M5/114.15.2), APC-Cy7/BUV737/FITC anti-mouse CD11b (clone M1/70), PE/BV421 anti-mouse XCR1 (clone ZET), BV421/BV786 anti-mouse CD103 (clone M290), APC-Cy7 anti-mouse CD24 (clone M1/69), BV605 anti-mouse CD8α (clone 53-6.7), APC/PE anti-mouse TLR3 (clone 11F8), BUV395 anti-mouse CD45 (clone 30-F11), PE-CF594 anti-mouse CD172a (SIRPα) (clone P84), APC anti-mouse ESAM (clone 1G8/ESAM), APC/PE anti-mouse IRF4 (clone 3E4), PerCP eF710 anti-mouse IRF8 (clone V3GYWCH), PE anti-mouse Clec9a (clone 7H11), FITC anti-mouse Vβ 5.1,5.2 (clone MR9-4), PerCp-Cy5.5 anti-mouse CD44 (clone IM7), PE anti-mouse CD45.2 (clone 104), Alexa Fluor® 647 anti-mouse Bcl-6 (clone K112-91), APC-Cy7 anti-mouse CD45.1 (clone A20), BUV395 anti-mouse CD4 (clone GK1.5), biotin anti-mouse CXCR5 (clone L138D7) and BUV737 streptavidin.

Splenic dendritic cell sorting and cDNA library preparation for RNA-seq

Splenic DCs were enriched using the Dynabeads Mouse DC Enrichment kit (Invitrogen), and sorted on a BD FACS Melody to obtain cDC1 ($B220^-CD64^-CD3^-CD19^-NK1.1^-CD11c^{hi}MHCII^+XCR1^+$) and cDC2 ($B220^-CD64^-CD3^-CD19^-NK1.1^-CD11c^{hi}MHCII^+CD11b^+XCR1^-$). Sorted cells (2-4x$10^4$ per sample) were resuspended in 350 μl RNeasy Lysis Buffer (QIAGEN), and RNA was extracted using the QIAGEN RNeasy Mini kit (QIAGEN). RNA was washed, treated with DNase I (QIAGEN), and eluted per the manufacturer's instructions. RNA Seq libraries were prepared by combining the Nugen Ovation RNA-seq system with NuGEN's Ovation RNA-Seq System V2 (NuGEN Technologies). The amplified libraries were purified using AMPure beads, quantified by qPCR, and visualized on an Agilent Bioanalyzer using BioA DNA High sensitivity (Agilent). The libraries were pooled equimolarly and run on a HiSeq 2500 as single end reads of 50 nucleotide length.

RNA sequencing data analysis

Sequencing reads were mapped to the mouse reference genome (GRCm38.85/mm10) using the STAR aligner (v2.7.6a)[49]. Alignments were guided by a Gene Transfer Format (Ensembl GTF GRCm38.101). Read count tables were normalized based on their library size factors using DESeq2 (v1.30.1)[50], and differential expression analysis was performed with a filter of log2foldChange >1 and a p-adjust value < 0.01. For selected gene signatures (cDC1 and cDC2 or ESAM^{hi} and ESAM^{lo} DC2s) the 100 DEGs with highest normalized count values were selected, out of which then the top 50 genes with highest absolute log2FoldChange were depicted in heatmaps. RNA-Seq reads aligned to genes from the GENCODE gene annotation were counted using Ensembl's BiomaRt-v2.46.3. Heatmap visualizations were done using pheatmap v1.0.12. Downstream statistical analyses and plot generation were performed in the R environment (v4.0.5).[51] The online tool Venny 2.1 was used for the drawing of the Venn plots.[52] Package PlotMA was used for visualizing of gene expression changes from two different conditions (parameters: alpha = 0.01, type =”ashr”).[53] Principal Component Analysis (PCA) plots were drawn using PCAtools 2.2.0, with removeVar=0.01.[54] Volcano plots were drawn using the function of ggpubr 0.4.0.[55] Gene Set Enrichment Analysis was performed using Gene Ontology R package clusterProfiler 3.18.1 (category biological process) on DEGs obtained from DESeq2. The p-values were adjusted using "BH" (Benjamini-Hochberg) correction and the cutoff was 0.01.[56] GO biological process terms were ranked by GeneRatio. The gene ratio is defined as the number of genes associated with the term in DEGs divided by the number of DEGs. For KEGG enrichment, DESeq2 derived DEGs were used.[57] Enrichments with a p-value from Fisher’s exact test ≤ 0.05 were considered significant.

Confocal Microscopy

Spleen and MLN were harvested, washed with cold DPBS and placed in 4% PFA for 12 hours, followed by an overnight wash with PBS-XG (PBS + 5% FCS + 0.2% Triton-X100 + 0.01% Thimerosal). Samples were embedded in warm 4% low melting agarose. 70-100µm sections were cut using a vibratome and stored until use. Samples were incubated with primary antibodies in

500ul PBS-XG in a 24 well plate overnight at 4°C under constant agitation (120rpm), followed by at least 6 hours of washing in 5ml PBS-XG. The following antibodies were used: BV421 anti-mouse B220/CD45R (clone RA3-6B2), APC anti-mouse TLR3 (clone 11F8), Alexa Fluor® 488 anti-mouse CD11c (clone N418) and PE-CF594 anti-mouse CD172a (SIRPα) (clone P84). Sections were mounted using ProLong Gold and images were acquired on a Zeiss LSM710 confocal microscope equipped with 488-, 561-, and 633-nm lasers and a tunable two photon laser. Digital pictures at 1,024 × 1,024-pixel density and 8-bit depth were acquired with ZEN software (Zeiss).

Cross presentation assay

Naïve CD8 T cells from OT-I donors were enriched using the Dynabeads® Untouched™ Mouse T Cells kit (Invitrogen) and stained in 1ml DPBS with CellTrace Violet dye (Invitrogen) for 10 min at 37°C. 1 x 10^6 OT-I cells were transferred into recipients one day before i.p. injection of 5 x 10^6 cells/mouse of H-2^{m1} MEFs expressing truncated non-secreted OVA (OVA-MEF).[17] 1 day after immunization, recipients were injected with FTY720 (20 µg/mouse; Cayman) in saline i.p.. Mice were sacrificed 3 days after immunization.

Generation of Follicular Helper T Cells *in vivo*

Naïve CD4 T cells from homozygote OT-II (CD45.1/.2) donors were enriched using the Dynabeads Untouched™ Mouse CD4 Cells kit (Invitrogen). 1 x 10^5 OT-II cells were transferred intravenously (i.v.) and 1 day later, recipients were immunized i.p. with ovalbumin grade V (OVA, 0.5 mg, Sigma Aldrich) together with poly(I:C) (100 µg, Sigma-Aldrich). Controls received PBS alone and mice were sacrificed 3 days after immunization.

Statistical Analysis

Statistical analyses were performed with Graphpad Prism 9.0 (Graphpad Software). One-way ANOVA with Tukey's correction for multiple comparisons was used. Significant differences are indicated as *P < 0.05, **P < 0.01, ***P < 0.001, and ****P < 0.0001.

Supplementary Materials

Supplementary Figure 1

Supplementary Table 1: Expression levels of top 50 DEGs between WT cDC1 and WT cDC2

Supplementary Table 2: DEGs between WT and *XCR.Bcl6*^{KO} cDC1 and WT and *CD11c.Bcl6*^{KO} cDC2

Supplementary Table 3: Expression levels of top 50 DEGs between ESAM^{hi} and ESAM^{lo} cDC2

Supplementary Table 4: Overlap of DEGs between WT and *CD11c.Bcl6*^{KO} cDC2 and ESAM^{lo} and ESAM^{hi} WT cDC2

References

1. Guilliams, M. *et al.* Dendritic cells, monocytes and macrophages: a unified nomenclature based on ontogeny. *Nat. Rev. Immunol.* **14**, 571–578 (2014).

2. Steinman, R. M. the Dendritic Cell System. *Annu. Rev. Immunol.* **9**, 271–296 (1991).

3. Durai, V. & Murphy, K. M. Functions of Murine Dendritic Cells. *Immunity* **45**, 719–736 (2016).

4. Allenspach, E. J., Lemos, M. P., Porrett, P. M., Turka, L. A. & Laufer, T. M. Migratory and Lymphoid-Resident Dendritic Cells Cooperate to Efficiently Prime Naive CD4 T cells. *Immunity* **29**, 795–806 (2008).

5. Lewis, S. M., Williams, A. & Eisenbarth, S. C. Structure and function of the immune system in the spleen. *Sci. Immunol.* **4**, (2019).

6. Eisenbarth, S. C. Dendritic cell subsets in T cell programming: location dictates function. *Nat. Rev. Immunol.* **19**, (2018).

7. Calabro, S. *et al.* Differential Intrasplenic Migration of Dendritic Cell Subsets Tailors Adaptive Immunity. *Cell Rep.* **16**, 2472–2485 (2016).

8. Idoyaga, J., Suda, N., Suda, K., Park, C. G. & Steinman, R. M. Antibody to Langerin/CD207 localizes large numbers of CD8α + dendritic cells to the marginal zone of mouse spleen. *Proc. Natl. Acad. Sci. U. S. A.* **106**, 1524–1529 (2009).

9. Sichien, D. *et al.* IRF8 Transcription Factor Controls Survival and Function of Terminally Differentiated Conventional and Plasmacytoid Dendritic Cells, Respectively. *Immunity* **45**, 626–640 (2016).

10. Schiavoni, G. *et al.* ICSBP is essential for the development of mouse type I interferon-producing cells and for the generation and activation of CD8α+ dendritic cells. *J. Exp. Med.* **196**, 1415–1425 (2002).

11. Hildner, K. *et al.* Batf3 deficiency reveals a critical role for CD8alpha+ dendritic cells in cytotoxic T cell immunity. *Science* **322**, 1097–1100 (2008).

12. Kashiwada, M., Pham, N. L. L., Pewe, L. L., Harty, J. T. & Rothman, P. B. NFIL3/E4BP4 is a key transcription factor for CD8α+ dendritic cell development. *Blood* **117**, 6193–6197 (2011).

13. Bagadia, P. *et al.* An Nfil3–Zeb2–Id2 pathway imposes Irf8 enhancer switching during cDC1 development. *Nat. Immunol.* **20**, 1174–1185 (2019).

14. Hacker, C. *et al.* Transcriptional profiling identifies Id2 function in dendritic cell development. *Nat. Immunol.* **4**, 380–386 (2003).

15. Cerovic, V. *et al.* Lymph-borne CD8α+ dendritic cells are uniquely able to cross-prime CD8+ T cells with antigen acquired from intestinal epithelial cells. *Mucosal Immunol.* **8**, 38–48 (2015).

16. Joeris, T. *et al.* Intestinal cDC1 drive cross-tolerance to epithelial-derived antigen via induction of FoxP3+CD8+ Tregs. *Sci. Immunol.* **6**, (2021).

17. Sancho, D. *et al.* Identification of a dendritic cell receptor that couples sensing of necrosis

to immunity. *Nature* **458**, 899–903 (2009).

18. Ahrens, S. *et al.* F-actin is an evolutionarily conserved damage-associated molecular pattern recognized by DNGR-1, a receptor for dead cells. *Immunity* **36**, 635–45 (2012).

19. Zhang, J.-G. *et al.* The dendritic cell receptor Clec9A binds damaged cells via exposed actin filaments. *Immunity* **36**, 646–57 (2012).

20. Satpathy, A. T. *et al.* Notch2-dependent classical dendritic cells orchestrate intestinal immunity to attaching-and-effacing bacterial pathogens. *Nat Immunol* **14**, 937–948 (2013).

21. Persson, E. K. *et al.* IRF4 transcription-factor-dependent CD103(+)CD11b(+) dendritic cells drive mucosal T helper 17 cell differentiation. *Immunity* **38**, 958–69 (2013).

22. Williams, J. W. *et al.* Transcription factor IRF4 drives dendritic cells to promote Th2 differentiation. *Nat Commun* **4**, 2990 (2013).

23. Scott, C. L. *et al.* The transcription factor Zeb2 regulates development of conventional and plasmacytoid DCs by repressing Id2. *J. Exp. Med.* jem.20151715 (2016). doi:10.1084/jem.20151715

24. Ichikawa, E. *et al.* Defective development of splenic and epidermal CD4+ dendritic cells in mice deficient for IFN regulatory factor-2. *Proc. Natl. Acad. Sci. U. S. A.* **101**, 3909–14 (2004).

25. Wu, L. *et al.* RelB is essential for the development of myeloid-related CD8alpha- dendritic cells but not of lymphoid-related CD8alpha+ dendritic cells. *Immunity* **9**, 839–47 (1998).

26. Lewis, K. L. *et al.* Notch2 receptor signaling controls functional differentiation of dendritic cells in the spleen and intestine. *Immunity* **35**, 780–791 (2011).

27. Briseño, C. G. *et al.* Notch2-dependent DC2s mediate splenic germinal center responses. *Proc. Natl. Acad. Sci. U. S. A.* **115**, 10726–10731 (2018).

28. Fasnacht, N. *et al.* Specific fibroblastic niches in secondary lymphoid organs orchestrate

distinct Notch-regulated immune responses. *J. Exp. Med.* **211**, 2265–2279 (2014).

29. Caton, M. L., Smith-Raska, M. R. & Reizis, B. Notch–RBP-J signaling controls the homeostasis of CD8 − dendritic cells in the spleen . *J. Exp. Med.* **204**, 1653–1664 (2007).

30. Lu, E., Dang, E. V., McDonald, J. G. & Cyster, J. G. Distinct oxysterol requirements for positioning naïve and activated dendritic cells in the spleen. *Sci. Immunol.* **2**, eaal5237 (2017).

31. Watchmaker, P. B. *et al.* Comparative transcriptional and functional profiling defines conserved programs of intestinal DC differentiation in humans and mice. *Nat. Immunol.* **15**, 98–108 (2014).

32. Tussiwand, R. *et al.* Klf4 Expression in Conventional Dendritic Cells Is Required for T Helper 2 Cell Responses. *Immunity* **42**, 916–928 (2015).

33. Brown, C. C. *et al.* Transcriptional Basis of Mouse and Human Dendritic Cell Heterogeneity. *Cell* **179**, 846-863.e24 (2019).

34. Choi, J. & Crotty, S. Bcl6-Mediated Transcriptional Regulation of Follicular Helper T cells (TFH). *Trends Immunol.* **42**, 336–349 (2021).

35. Ohtsuka, H. *et al.* Bcl6 Is Required for the Development of Mouse CD4+ and CD8 + Dendritic Cells. *J. Immunol.* **186**, 255–263 (2011).

36. Bagadia, P. *et al.* Bcl6 -Independent In Vivo Development of Functional Type 1 Classical Dendritic Cells Supporting Tumor Rejection . *J. Immunol.* ji1901010 (2021). doi:10.4049/jimmunol.1901010

37. Schraml, B. U. *et al.* Genetic tracing via DNGR-1 expression history defines dendritic cells as a hematopoietic lineage. *Cell* **154**, 843–858 (2013).

38. Lau, C. M. *et al.* Leukemia-associated activating mutation of Flt3 expands dendritic cells and alters T cell responses. *J. Exp. Med.* **213**, 415–431 (2016).

39. Baumjohann, D., Okada, T. & Ansel, K. M. Cutting Edge: Distinct Waves of BCL6

Expression during T Follicular Helper Cell Development. *J. Immunol.* **187**, 2089–2092 (2011).

40. Baumjohann, D. *et al.* Persistent Antigen and Germinal Center B Cells Sustain T Follicular Helper Cell Responses and Phenotype. *Immunity* **38**, 596–605 (2013).

41. Zhang, S. *et al.* Type 1 conventional dendritic cell fate and function are controlled by DC-SCRIPT. *Sci. Immunol.* **6**, (2021).

42. Zhang, T. T. *et al.* Dynamic expression of BCl6 in murine conventional dendritic cells during in vivo development and activation. *PLoS One* **9**, 1–12 (2014).

43. Gatto, D. *et al.* The chemotactic receptor EBI2 regulates the homeostasis, localization and immunological function of splenic dendritic cells. *Nat. Immunol.* **14**, 446–453 (2013).

44. Yi, T. & Cyster, J. G. EBI2-mediated bridging channel positioning supports splenic dendritic cell homeostasis and particulate antigen capture. *Elife* **2**, e00757 (2013).

45. Durai, V. *et al.* Cryptic activation of an Irf8 enhancer governs cDC1 fate specification. *Nat. Immunol.* **20**, 1161–1173 (2019).

46. Wohn, C. *et al.* Absence of MHC class II on cDC1 dendritic cells triggers fatal autoimmunity to a cross-presented self-antigen. *Sci. Immunol.* **5**, (2020).

47. Hollister, K. *et al.* Insights into the Role of Bcl6 in Follicular Th Cells Using a New Conditional Mutant Mouse Model. *J. Immunol.* **191**, 3705–3711 (2013).

48. Johansson-Lindbom, B. *et al.* Functional specialization of gut CD103 + dendritic cells in the regulation of tissue-selective T cell homing . *J. Exp. Med.* **202**, 1063–1073 (2005).

49. Dobin, A. *et al.* STAR: Ultrafast universal RNA-seq aligner. *Bioinformatics* **29**, 15–21 (2013).

50. Love, M. I., Huber, W. & Anders, S. Moderated estimation of fold change and dispersion for RNA-seq data with DESeq2. *Genome Biol.* **15**, (2014).

51. R Core Team (2020). R: A language and environment for statistical computing. R

Foundation for Statistical Computing, Vienna, Austria. (2020).

52. Oliveros, J. C. Venny. An Interactive Tool for Comparing Lists with Venn's Diagrams.

53. Stephens, M. False discovery rates: A new deal. *Biostatistics* **18**, 275–294 (2017).

54. Blighe, K. and A. L. PCAtools: everything Principal Components Analysis.https://github.com/kevinblighe/PCAtools. (2019).

55. Alboukadel Kassambara. ggpubr:'ggplot2' Based Publication Ready Plots. (2020).

56. Yu, G., Wang, L.-G., Han, Y. & He, Q.-Y. clusterProfiler: an R Package for Comparing Biological Themes Among Gene Clusters. *Omi. A J. Integr. Biol.* **16**, (2012).

57. Qiu, Y.-Q. KEGG Pathway Database. in *Encyclopedia of Systems Biology* (eds. Dubitzky, W., Wolkenhauer, O., Cho, K.-H. & Yokota, H.) 1068–1069 (Springer New York, 2013). doi:10.1007/978-1-4419-9863-7_472

Acknowledgements

We thank Katrine Fog Starup and Julien Vandamme for excellent technical support, the Lahl, Agace and Bekiaris laboratories for fruitful discussions, and Prof Allan Mowat for intellectual input and manuscript editing. The *Bcl6*$^{fl/fl}$ mice were kindly gifted by Alexander Dent and the OVA-MEF line was from Caetano Reis e Sousa.

Funding

China Scholarship Council fellowship (HX)
Lundbeck Foundation Fellowship R215-2015-4100 (KL)
Ragnar Söderberg Foundation Fellowship in Medicine (KL)
Vetenskapsrådet 2020-01977 (KL)
Cancerfonden 21 1826 Pj (KL)
Novo Nordisk Foundation 18038 (KL)
Crafoord Foundation (KL)
European Research Council ERC-2016-STG-715182 (BS)

Deutsche Forschungsgemeinschaft (DFG, German Research Foundation) Emmy Noether grant Schr 1444/1-1, Project-ID 360372040 – SFB 1335 (project 8) and 322359157-FOR2599-A03 (BS)
Deutsche Forschungsgemeinschaft (DFG, German Research Foundation) Emmy Noether Programme BA 5132/1-2 (252623821), SFB 1054 Project B12 (210592381) (DB)
Germany's Excellence Strategy EXC2151 (390873048) (DB).

Author Contributions:

Conceptualization: KL

Methodology: HX, IU, HN, IK, UM, DB, FP, BUS, KL

Investigation: HX, IU, HN, IK, UM, KL

Visualization: HX, UM, KL

Funding acquisition: HX, DB, BUS, KL

Project administration: KL

Supervision: FP, BUS, KL

Writing – original draft: KL

Writing – review & editing: BUS, KL

Competing Interests

Authors declare that they have no competing interests

Data Availability

Raw RNA-sequencing data files are accessible through the NCBI SRA database under the accession number PRJNA834905.

Figures:

Fig. 1.

A. Left: Splenic XCR1^{+} and XCR1^{-}CD11b^{+} DC subsets in wt (black), *XCR1.Bcl6^{KO}* (orange), and *CD11c.Bcl6^{KO}* (red) mice. Plots show representative staining profiles of gated live, single lineage^{-}

(CD3, CD19, CD64, B220, NK1.1), MHCII$^+$, CD11c^{hi} splenocytes. Right: Absolute numbers of splenic XCR1$^+$ and XCR1$^-$CD11b$^+$ DC from wt, *XCR1.Bcl6^{KO}*, and *CD11c.Bcl6^{KO}* mice. Statistical analysis by one-way ANOVA. * P<0.01 and ** P<0.001. Data points represent values from individual mice pooled from 8-9 experiments and lines represent the medians.

B. Left: Flow cytometry plots showing resident XCR1$^+$ and XCR1$^-$CD11b$^+$ DC subsets in the pLNs and mLNs of wt, *XCR1.Bcl6^{KO}*, and *CD11c.Bcl6^{KO}* mice. Plots show representative staining profiles of gated single live, CD45$^+$, lineage$^-$ (CD3, CD19, CD64, B220, NK1.1), CD11c^{hi}MHCII^{int} resident DCs. Right: Absolute numbers of resident cDC subsets in the pLN and mLN of wt, *XCR1.Bcl6^{KO}*, and *CD11c.Bcl6^{KO}* mice. Statistical analysis by one-way ANOVA. * P<0.05. Data points represent values from individual mice pooled from at least 4 experiments and lines represent the medians.

Fig. 2.

A. Left: Flow cytometry plots showing migratory XCR1$^+$ and XCR1$^-$CD11b$^+$ DC subsets in the pLN (top) and mLN (middle) of wt (black), *XCR1.Bcl6^{KO}* (orange), and *CD11c.Bcl6^{KO}* (red) mice. mLN XCR1$^-$ DCs are further sub-divided into CD103$^+$ and CD103$^-$ (bottom). Plots show representative staining profiles of live single, CD45$^+$, lineage$^-$ (CD3, CD19, CD64, B220, NK1.1), CD11c^{int}MHCII^{hi} migratory DCs. Right: Absolute numbers of migratory cDC subsets from pLN and mLN of wt, *XCR1.Bcl6^{KO}*, and *CD11c.Bcl6^{KO}* mice. Statistical analysis by one-way ANOVA. * P<0.05, ** P<0.01, *** P<0.001 and **** P<0.0001. Data points represent values from individual mice pooled from at least 4 experiments and lines represent the medians.

B. Left: Flow cytometry plots showing small intestinal lamina propria XCR1$^+$ and XCR1$^-$CD11b$^+$ DC subsets from wt, *XCR1.Bcl6^{KO}*, and *CD11c.Bcl6^{KO}* mice. Plots show representative staining profiles of live, CD45$^+$, lineage$^-$ (CD3, CD19, CD64, B220, NK1.1), MHCII$^+$, CD11c^{hi} gated single cells.
Right: Absolute numbers of XCR1$^+$ and XCR1$^-$CD11b$^+$ DC subsets from wt, *XCR1.Bcl6^{KO}*, and *CD11c.Bcl6^{KO}* mice. Statistical analysis was performed by one-way ANOVA.* P<0.05 and ** P<0.01. Data points represent values from individual mice pooled from 3 experiments and lines represent the medians.

C. Representative FACS plots showing small intestinal lamina propria XCR1$^+$ and XCR1$^-$CD11b$^+$ DC subsets from wt and *Clec9α.Bcl6^{KO}* mice, left: gated on all DCs (live, CD45$^+$, CD64$^-$, Ly6C$^-$, MHCII$^+$, CD11c^{hi} single cells); right: Additionally gated on XCR1$^-$, pre-gated on YFP$^+$ in green and on YFP$^-$ in blue. The quantification on the right depicts % CD103+CD11b+XCR1- cDC2 out of all cDC2 in the

YFP$^+$ vs YFP$^-$ population. Statistical analysis was performed by paired T Test, * P<0.05. Data points represent values from individual mice pooled from 2 experiments with 2 mice each.

Fig. 3.

A. Principal component analysis (PCA) plot of gene expression data obtained from bulk RNA-seq using DESeq2. Color coded icons show cDC1 and cDC2 from the spleen of wt, *XCR1.Bcl6^{KO}*, and *XCR1.Bcl6^{KO}* mice. Three replicates were included in each group.
B. Heatmap of selected highly expressed cDC1 or cDC2 associated genes in all RNA-Seq samples (50 most differentially expressed genes between cDC1 and cDC2 chosen from the 100 genes with highest expression level among total differentially expressed genes (fold change $\geqslant$ 2, padj: 0.01) in wt samples). The color scale represents the row Z score.
C. Volcano plots showing the global transcriptional differences between splenic cDC2 and cDC1 in wt (left), *XCR1.Bcl6^{KO}* (middle) and *CD11c.Bcl6^{KO}* mice (right). Each circle represents one gene. The log2FoldChange (LFC) is represented on the x-axis. The y-axis shows the –(log10 of the p adjust value). A padj value of 0.01 and an absolute LFC of 1 are indicated by dashed lines. The upregulated or downregulated genes are shown in red or blue dots respectively, and the top ranked gene symbols with the lowest padj value were annotated in the plot.
D. VENN diagram showing significantly elevated differentially expressed genes (DEGs) (|Log2foldchange|$\geqslant$1 and padj<0.01) between *XCR1.Bcl6^{KO}* cDC1 (red) and wt cDC1 (blue), and between *CD11c.Bcl6^{KO}* cDC2 (orange) and wt cDC2 (green).

Fig. 4.

A. Flow cytometric analysis of cDC1 in spleen of wt and *XCR1.Bcl6^{KO}* mice. Representative histograms show indicated protein expression on wt (black) and *XCR1.Bcl6^{KO}* (red), with FMO staining shown in grey. Pre-gating on cDC1 was performed as in 1A. Data are representative of two independent experiments with 2-3 mice each.
B. Gene ontology (GO) term enrichment analysis of differentially expressed genes (DEGs) in *XCR1.Bcl6^{KO}* and wt cDC1. The p value calculated from GO term enrichment analysis is represented on the x-axis and the y-axis shows the GO Biological Process (BP) terms.

C. KEGG (Kyoto Encyclopedia of Genes and Genomes) term enrichment analysis of DEGs in *XCR1.Bcl6*^{KO} vs wt cDC1. The GeneRatio value calculated from KEGG term enrichment analysis is represented on the x-axis and the y-axis shows the KEGG enriched terms.

D. Heatmap of all genes contributing to the enriched KEGG pathways depicted in B. The color scale represents the row Z score.

Fig. 5.

A. Representative flow cytometry plots showing VCT and CD44 expression on OT-I cells (gated on live, CD3^{+}CD8^{+}CD45.1^{+} single cells) in the spleen (top) and mLN (bottom) of wt and *XCR1.Bcl6*^{KO} recipient mice 3 days after i.p. immunization with heat shocked OVA-MEFs. Data are representative of three independent experiments with 2-5 mice each.

B. Total number of OT I cells in the spleen (right) and mLN (left) of immunized wt and *XCR1.Bcl6*^{KO} mice. Data are pooled from 3 independent experiments. Each dot represents one mouse and lines represent the medians. *$p<0.05$, ns, not significant.

Fig. 6.

A. Representative flow cytometric analysis of cDC2 in the spleen of wt and *CD11c.Bcl6*^{KO} mice, showing expression of CD11c vs MHCII (top panels) and XCR1 vs CD11b (lower panels) by live, lineage^{-} (CD3, CD19, CD64, B220, NK1.1) single cell-gated splenocytes. Data are representative of at least 8 independent experiments with 1 – 3 mice each.

B. Representative flow cytometric analysis of ESAM^{hi} and ESAM^{lo} cDC2 in the spleen of wt and *CD11c.Bcl6*^{KO} mice. Cells were pre-gated as XCR1^{-}CD11b^{+} cDC2 from live, lineage^{-} (CD3, CD19, CD64, B220, NK1.1) single cells. Data are representative of three independent experiments with 1 – 3 mice each.

C. Representative flow cytometric analysis of cDC2 in the spleen of wt and *Clec9a.Bcl6*^{KO} mice, showing expression of CD11c vs MHCII (top panels) and XCR1 vs CD11b (lower panels) by live, lineage^{-} (CD3, CD19, CD64, B220, NK1.1) single cell-gated splenocytes. Data are representative of two independent experiments with 3 mice each.

D. Representative flow cytometric analysis of ESAM^{hi} and ESAM^{lo} cDC2 in the spleen of wt and *Clec9a.Bcl6*^{KO} mice. Cells were pre-gated as XCR1^{-}CD11b^{+} cDC2 from live, lineage^{-} (CD3, CD19,

CD64, B220, NK1.1) single cells (top). Data are representative of two independent experiments with 3 mice each. Bottom plots were pre-gated on YFP^+ cells to enrich for cDC2 with a history of Clec9A-promoter activity.

E. Representative flow cytometric analysis of the CD11c, 33D1, CD4, CD11b and IRF4 by splenic $XCR1^-$ $CD11b^+$ cDC2 from wt or *CD11c.Bcl6*^{KO} mice. Gates correspond to those depicted in Fig. 6B. Results are representative of at least two (IRF4) or three (all others) independent experiments with 1 - 3 mice each.

Fig. 7.

A. The top 50 genes associated with spleen $ESAM^{hi}$ cDC2 (left) or $ESAM^{lo}$ cDC2 (right) were derived from GSE76132. Heatmaps show the expression of these genes in the RNA-Seq analysis of cDC2 from wt and *CD11c.Bcl6*^{KO} spleen. The color scale represents the row Z score (Expression Z-scale).

B. VENN diagram showing significantly elevated DEGs (|Log2foldchange| $\geqslant$1 and padj<0.01) in cDC2 from *CD11c.Bcl6*^{KO} (orange) and wt (green) mice (our RNA-Seq dataset), together with wt $ESAM^{hi}$ (yellow) and wt $ESAM^{hi}$ (blue) cDC2 (GSE76132 dataset).

C. Confocal microscopy of spleens from *CD11c.Bcl6*^{KO} and wt mice showing expression of TLR3 (grey: upper left quadrant), CD11c (green: upper right quadrant), Sirpα (red: lower left quandrant) and B220 (blue: lower right quadrant). Scale bar=50μm. Orange arrows indicate marginal zone bridging channels. The images shown are from one out of four (*CD11c.Bcl6*^{KO}) or three (wt) replicates derived from individual mice.

D. Representative flow cytometric analysis of early T_{FH} cell induction amongst OT-II cells in the spleen of wt and *CD11c.Bcl6*^{KO} mice 3 days after i.p. immunization with OVA and poly(I:C) or with PBS as a control. T_{FH} were ga6ed as live, $CD4^+V\beta5.2^+CD45.1^+CD45.2^+CD44^+Bcl6^+CXCR5^+$ and the results are representative of three experiments with 3-5 mice each. Each experiment contained at least one unimmunized (PBS) control per genotype.

E. Numbers of total OT-II T cells (left panel), together with absolute numbers (middle panel) and proportions (right panel) of OVA-specific T_{FH} cells in the spleens of wt and *CD11c.Bcl6*^{KO} mice 3 days after i.p. immunization with OVA and poly(I:C) or with PBS as a control. Statistical analysis was performed by one-way ANOVA. * P<0.05, ** P<0.01, *** P<0.001 and **** P<0.0001. Data points represent values from individual mice pooled from three experiments with 3-5 mice each in OVA/poly(I:C) immunized groups. Each experiment contained at least one untreated control per genotype; lines represent the medians.

Supplementary Figure 1

A. Left: Flow cytometry plots show XCR1^{+} and XCR1^{-}CD11b^{+} DC subsets in the lungs of wt, *XCR1.Bcl6^{KO}* and *CD11c.Bcl6^{KO}* mice. The plots show representative staining profiles of live, CD45^{+}, lineage^{-} (CD3, CD19, CD64, B220, NK1.1), MHCII^{+}, CD11c^{hi} gated single cells. Right: Absolute numbers of cDC subsets in the lungs of wt, *XCR1.Bcl6^{KO}*, and *CD11c.Bcl6^{KO}* mice. Statistical analysis by one-way ANOVA.** P<0.01, **** P<0.0001. Data points represent values from individual mice pooled from 2-3 experiments and lines represent the medians.
B. Left: Representative flow cytometry plots on blood XCR1^{+} and XCR1^{-}CD11b^{+} DC subsets from wt, XCR1.Bcl6^{KO} and CD11c.Bcl6^{KO}. Shown are representative staining profiles of live, CD45^{+}, lineage^{-} (CD3, CD19, CD64, B220, NK1.1), MHCII^{+}, CD11c^{hi} gated single cells. Right: Quantification of blood cDC1 and cDC2 absolute numbers from wt, XCR1.Bcl6^{KO}, and CD11c.Bcl6^{KO} mice. Statistical analysis by one-way ANOVA. Significance at * P<0.05. Data points are normalized to volume of blood drawn and represent values from individual mice pooled from 4 experiments; lines represent the median cell numbers from each genotype.

Figure 1

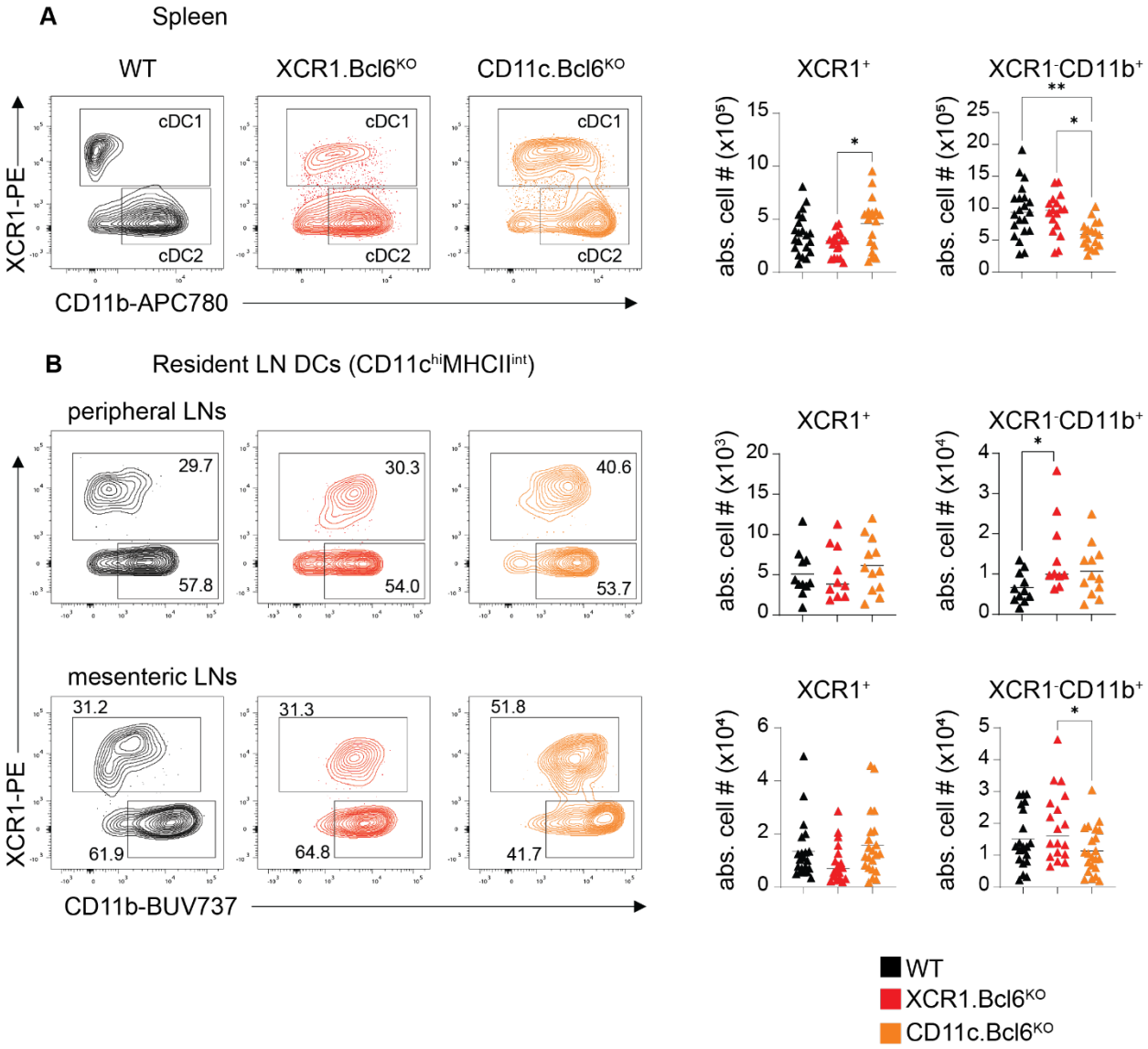
A
Spleen
WT
XCR1.Bcl6KO
CD11c.Bcl6KO
cDC1
cDC2
XCR1-PE
CD11b-APC780
XCR1+
XCR1-CD11b+
abs. cell # (x10^5)
B
Resident LN DCs (CD11chiMHCIIint)
peripheral LNs
29.7
57.8
30.3
54.0
40.6
53.7
mesenteric LNs
31.2
61.9
31.3
64.8
51.8
41.7
CD11b-BUV737
abs. cell # (x10^3)
abs. cell # (x10^4)
WT
XCR1.Bcl6KO
CD11c.Bcl6KO

Figure 2

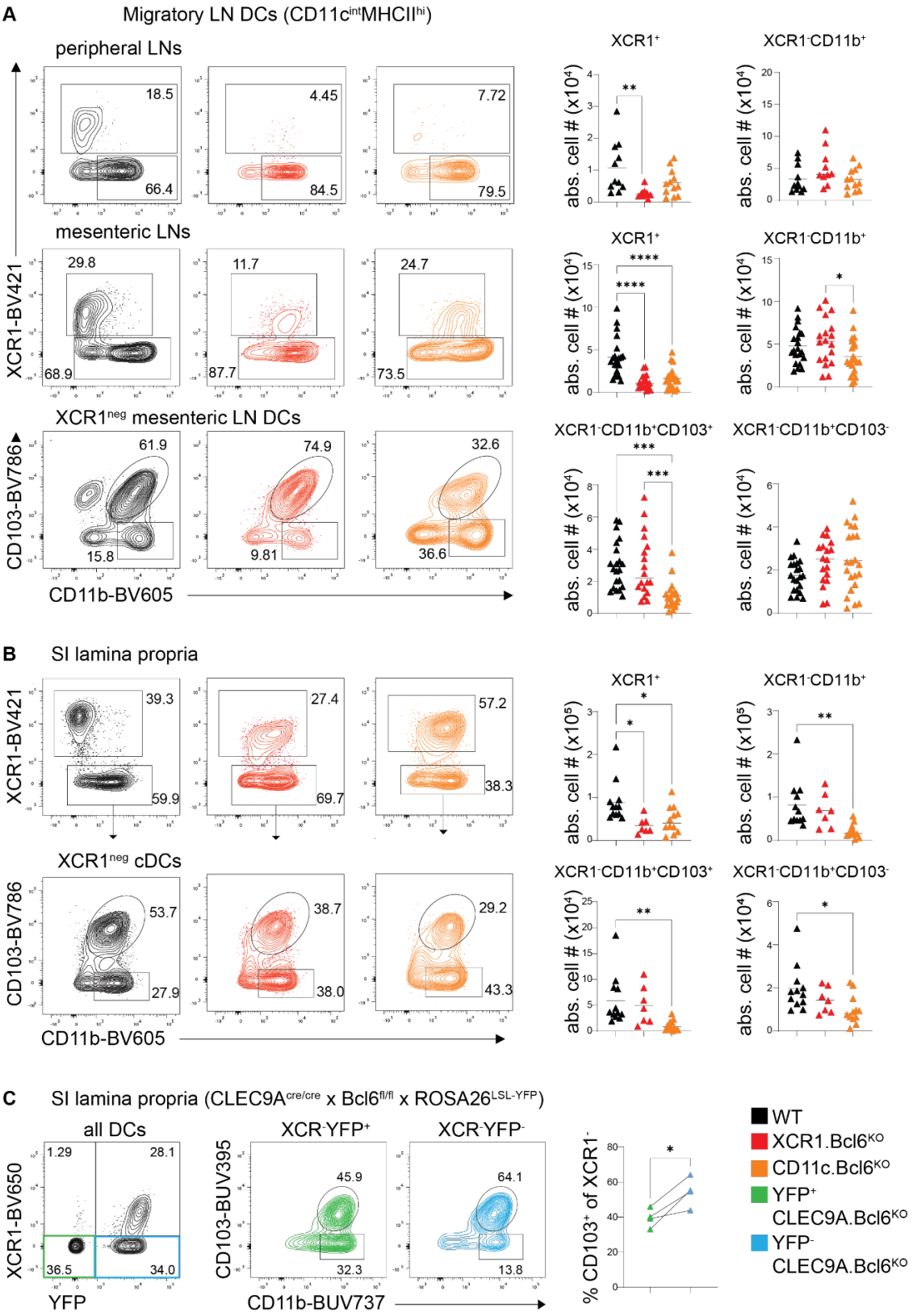
A
Migratory LN DCs (CD11c^intMHCII^hi)
peripheral LNs
mesenteric LNs
XCR1-BV421
XCR1^neg mesenteric LN DCs
CD103-BV786
CD11b-BV605
XCR1+
XCR1-CD11b+
XCR1-CD11b+CD103+
XCR1-CD11b+CD103-
abs. cell # (x10^4)
B
SI lamina propria
XCR1^neg cDCs
abs. cell # (x10^5)
C
SI lamina propria (CLEC9A^cre/cre x Bcl6^fl/fl x ROSA26^LSL-YFP)
all DCs
XCR-YFP+
XCR-YFP-
XCR1-BV650
CD103-BUV395
CD11b-BUV737
YFP
% CD103+ of XCR1-
WT
XCR1.Bcl6^KO
CD11c.Bcl6^KO
YFP+ CLEC9A.Bcl6^KO
YFP- CLEC9A.Bcl6^KO

Figure 3

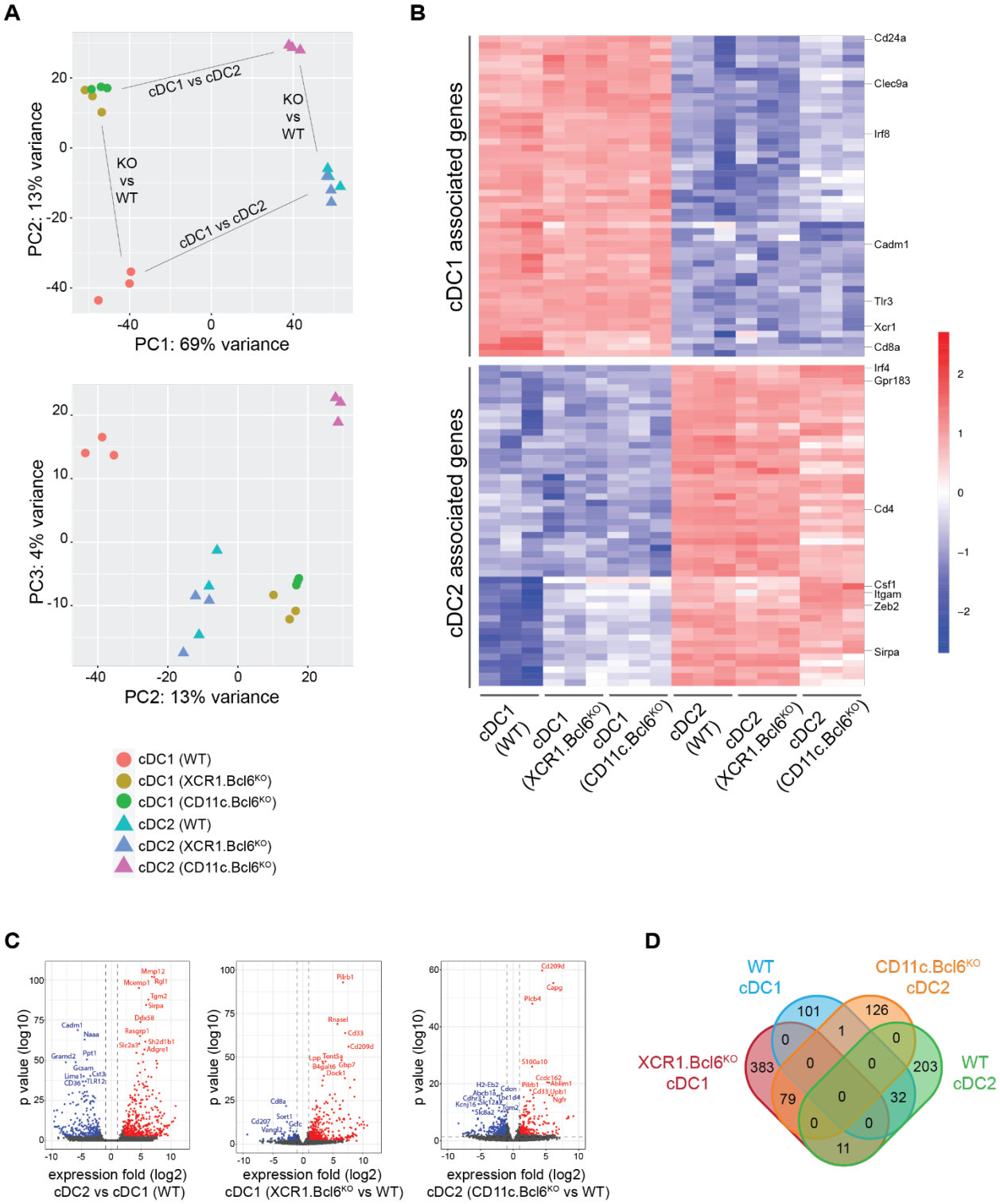
A
B
C
D
cDC1 vs cDC2
KO vs WT
KO vs WT
cDC1 vs cDC2
PC2: 13% variance
PC1: 69% variance
PC3: 4% variance
PC2: 13% variance
cDC1 (WT)
cDC1 (XCR1.Bcl6KO)
cDC1 (CD11c.Bcl6KO)
cDC2 (WT)
cDC2 (XCR1.Bcl6KO)
cDC2 (CD11c.Bcl6KO)
cDC1 associated genes
cDC2 associated genes
Cd24a
Clec9a
Irf8
Cadm1
Tlr3
Xcr1
Cd8a
Irf4
Gpr183
Cd4
Csf1
Itgam
Zeb2
Sirpa
cDC1 (WT)
cDC1 (XCR1.Bcl6KO)
cDC1 (CD11c.Bcl6KO)
cDC2 (WT)
cDC2 (XCR1.Bcl6KO)
cDC2 (CD11c.Bcl6KO)
p value (log10)
expression fold (log2)
cDC2 vs cDC1 (WT)
cDC1 (XCR1.Bcl6KO vs WT)
cDC2 (CD11c.Bcl6KO vs WT)
WT cDC1
CD11c.Bcl6KO cDC2
XCR1.Bcl6KO cDC1
WT cDC2
101
126
1
0
0
383
0
0
203
79
0
32
0
0
11

Figure 4

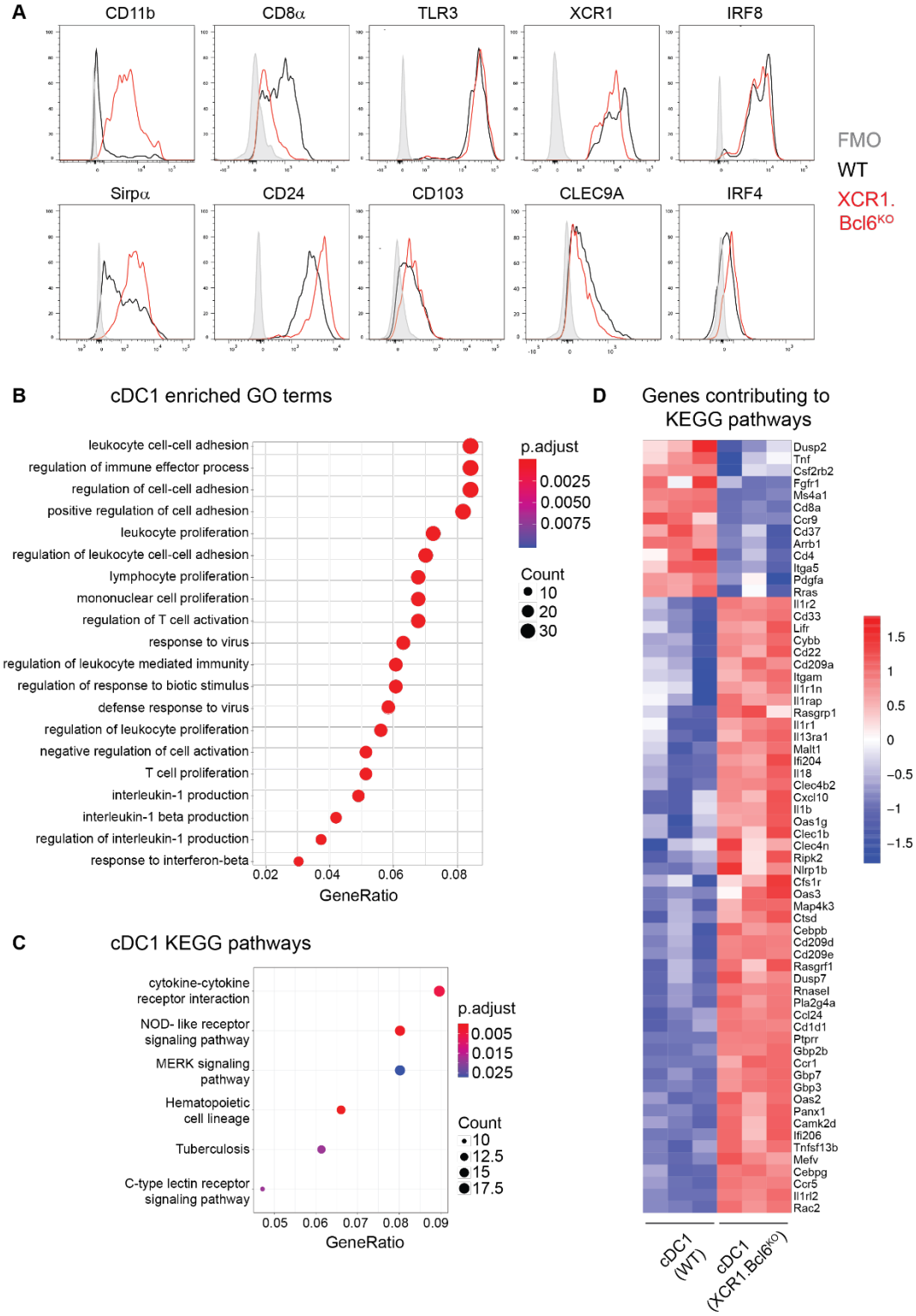
A
CD11b
CD8α
TLR3
XCR1
IRF8
Sirpα
CD24
CD103
CLEC9A
IRF4
FMO
WT
XCR1.
Bcl6KO
B
cDC1 enriched GO terms
leukocyte cell-cell adhesion
regulation of immune effector process
regulation of cell-cell adhesion
positive regulation of cell adhesion
leukocyte proliferation
regulation of leukocyte cell-cell adhesion
lymphocyte proliferation
mononuclear cell proliferation
regulation of T cell activation
response to virus
regulation of leukocyte mediated immunity
regulation of response to biotic stimulus
defense response to virus
regulation of leukocyte proliferation
negative regulation of cell activation
T cell proliferation
interleukin-1 production
interleukin-1 beta production
regulation of interleukin-1 production
response to interferon-beta
0.02
0.04
0.06
0.08
GeneRatio
p.adjust
0.0025
0.0050
0.0075
Count
10
20
30
C
cDC1 KEGG pathways
cytokine-cytokine receptor interaction
NOD- like receptor signaling pathway
MERK signaling pathway
Hematopoietic cell lineage
Tuberculosis
C-type lectin receptor signaling pathway
0.05
0.06
0.07
0.08
0.09
GeneRatio
p.adjust
0.005
0.015
0.025
Count
10
12.5
15
17.5
D
Genes contributing to KEGG pathways
Dusp2
Tnf
Csf2rb2
Fgfr1
Ms4a1
Cd8a
Ccr9
Cd37
Arrb1
Cd4
Itga5
Pdgfa
Rras
Il1r2
Cd33
Lifr
Cybb
Cd22
Cd209a
Itgam
Il1r1n
Il1rap
Rasgrp1
Il1r1
Il13ra1
Malt1
Ifi204
Il18
Clec4b2
Cxcl10
Il1b
Oas1g
Clec1b
Clec4n
Ripk2
Nlrp1b
Cfs1r
Oas3
Map4k3
Ctsd
Cebpb
Cd209d
Cd209e
Rasgrf1
Dusp7
RnaseI
Pla2g4a
Ccl24
Cd1d1
Ptprr
Gbp2b
Ccr1
Gbp7
Gbp3
Oas2
Panx1
Camk2d
Ifi206
Tnfsf13b
Mefv
Cebpg
Ccr5
Il1rl2
Rac2
1.5
1
0.5
0
−0.5
−1
−1.5
cDC1 (WT)
cDC1 (XCR1.Bcl6KO)

Figure 5

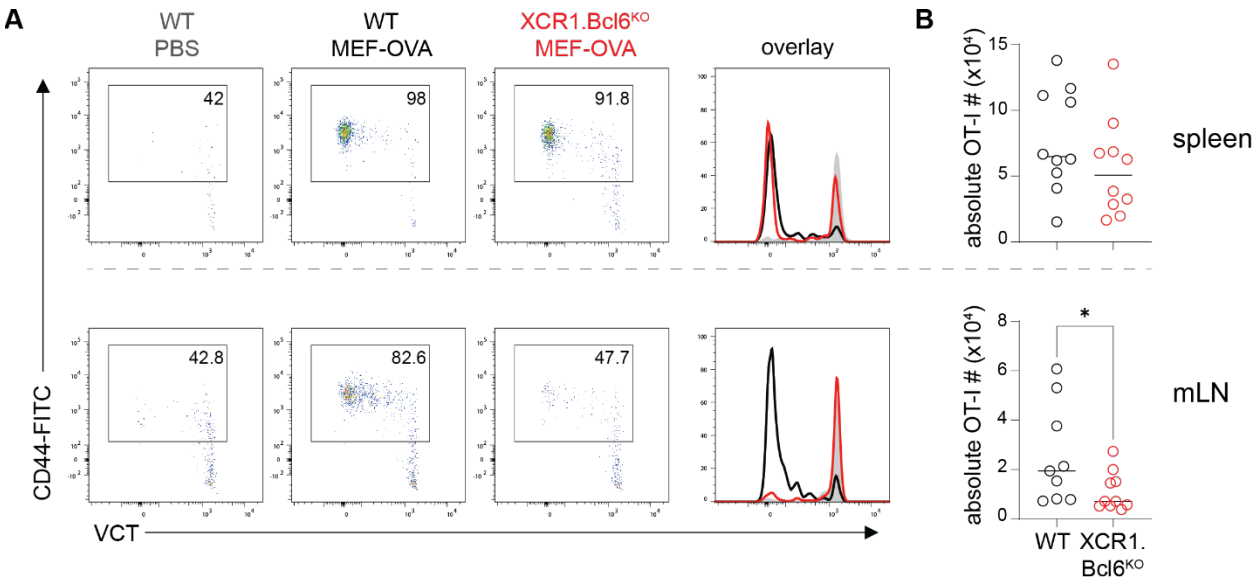
A
WT
PBS
WT
MEF-OVA
XCR1.Bcl6KO
MEF-OVA
overlay
42
98
91.8
42.8
82.6
47.7
CD44-FITC
VCT
B
absolute OT-I # (x10⁴)
spleen
mLN
*
WT
XCR1.
Bcl6KO

Figure 6

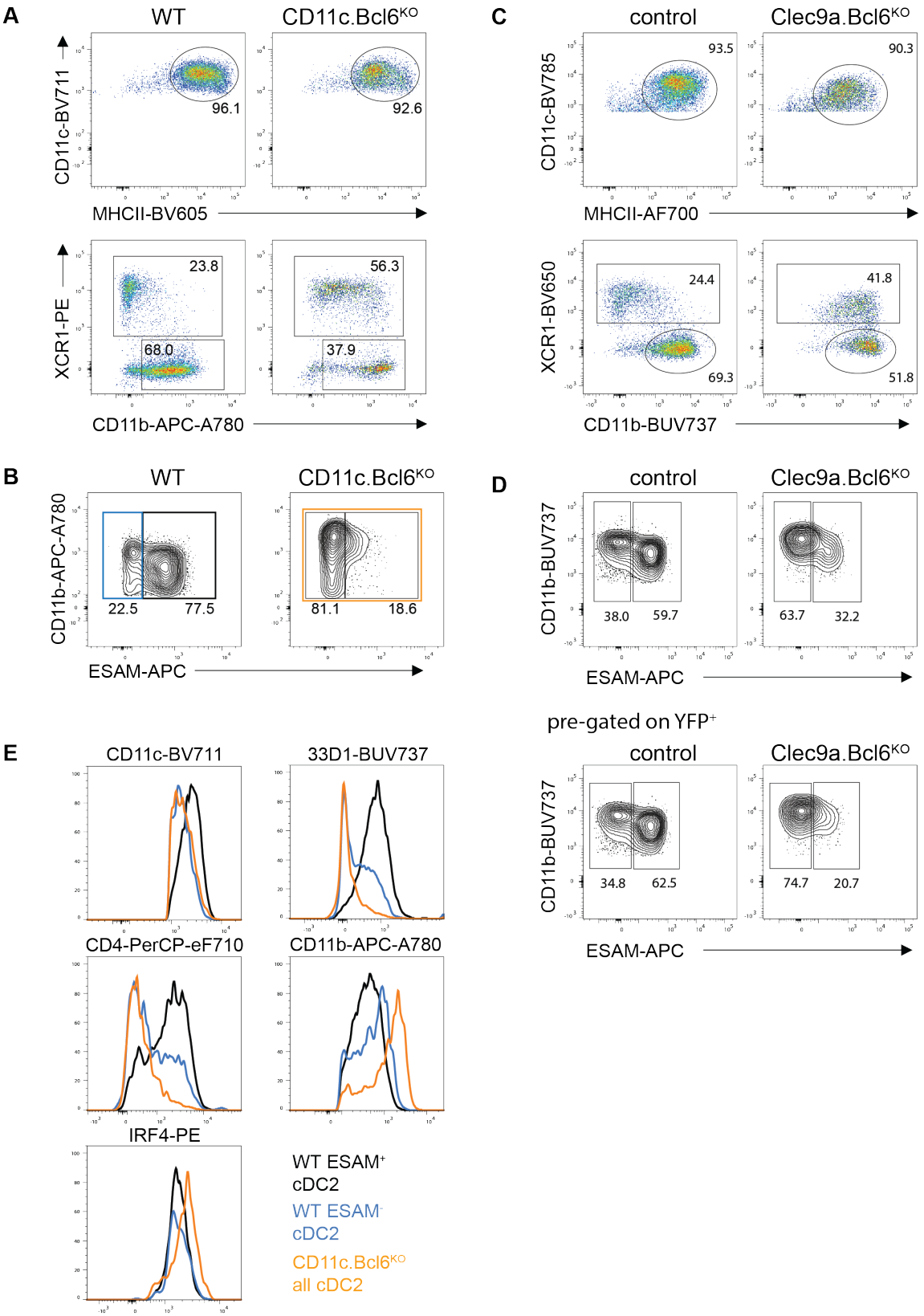
A
WT
CD11c.Bcl6KO
CD11c-BV711
MHCII-BV605
96.1
92.6
XCR1-PE
CD11b-APC-A780
23.8
68.0
56.3
37.9
B
WT
CD11c.Bcl6KO
CD11b-APC-A780
ESAM-APC
22.5
77.5
81.1
18.6
C
control
Clec9a.Bcl6KO
CD11c-BV785
MHCII-AF700
93.5
90.3
XCR1-BV650
CD11b-BUV737
24.4
69.3
41.8
51.8
D
control
Clec9a.Bcl6KO
CD11b-BUV737
ESAM-APC
38.0
59.7
63.7
32.2
pre-gated on YFP+
control
Clec9a.Bcl6KO
CD11b-BUV737
ESAM-APC
34.8
62.5
74.7
20.7
E
CD11c-BV711
33D1-BUV737
CD4-PerCP-eF710
CD11b-APC-A780
IRF4-PE
WT ESAM+ cDC2
WT ESAM- cDC2
CD11c.Bcl6KO all cDC2

Figure 7

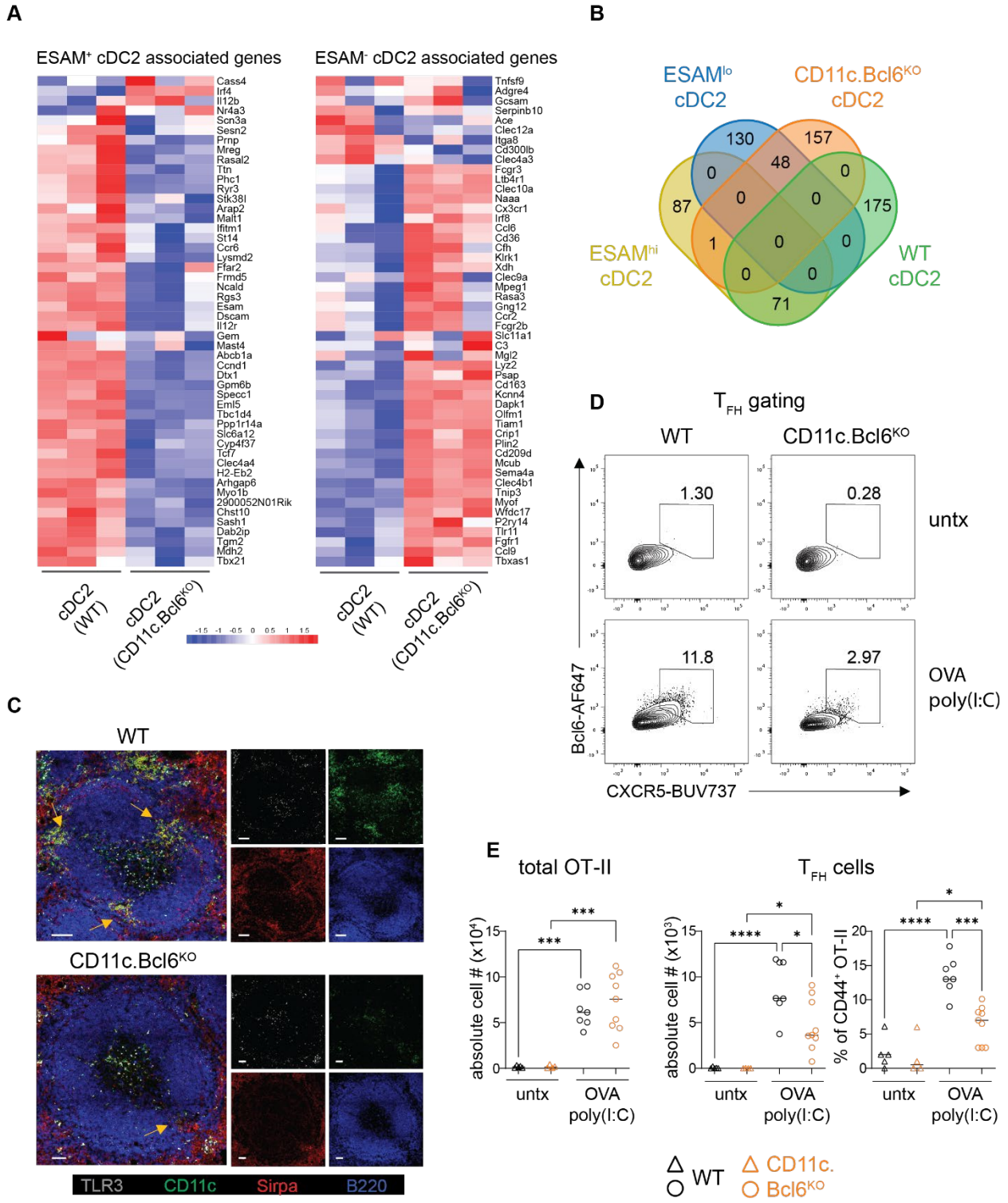
A
ESAM+ cDC2 associated genes
ESAM- cDC2 associated genes
cDC2 (WT)
cDC2 (CD11c.Bcl6KO)
B
ESAMlo cDC2
CD11c.Bcl6KO cDC2
ESAMhi cDC2
WT cDC2
130
157
48
87
175
71
D
TFH gating
WT
CD11c.Bcl6KO
untx
OVA poly(I:C)
1.30
0.28
11.8
2.97
Bcl6-AF647
CXCR5-BUV737
C
WT
CD11c.Bcl6KO
TLR3
CD11c
Sirpa
B220
E
total OT-II
TFH cells
absolute cell # (x10^4)
absolute cell # (x10^3)
% of CD44+ OT-II
untx
OVA poly(I:C)
WT
CD11c. Bcl6KO